Supporting information for:

Strong pH-Dependent Near-Infrared Fluorescence in a Microbial Rhodopsin Reconstituted with a Red-Shifting Retinal Analogue

Yusaku Hontani[†], *Srividya Ganapathy*[‡], *Sean Frehan*[†], *Miroslav Kloz*[†#], *Willem J. de Grip*[‡¶] *and John T.M. Kennis*[†*]

[†] Department of Physics and Astronomy, Vrije Universiteit, Amsterdam 1081 HV, The Netherlands.

[‡]Department of Biophysical Organic Chemistry, Leiden Institute of Chemistry, Gorlaeus Laboratories, Leiden University, Leiden 2300 RA, The Netherlands

[#] ELI-Beamlines, Institute of Physics, Na Slovance 2, 182 21 Praha 8, Czech Republic

[¶]Department of Biochemistry, Radboud University Medical Center, Nijmegen 6500 HB, The Netherlands.

Methods

Cell culturing: E. coli strain UT5600 transformed with the pKJ900 plasmid was used to express recombinant PR with a C-terminal 6-His tag. The cells were grown in LB medium, harvested, lysed and regenerated with the appropriate retinal as per protocols described previously [1-2].

Protein purification: The lysed cell suspension was incubated with 4% DDM (w/v) overnight at 4°C and centrifuged to remove the insoluble cellular debris. The His-tagged proteorhodopsins were purified by immobilized-metal affinity chromatography (IMAC), as reported previously [2]. 10 ml Ni^{2+}-NTA resin was used per 2000 mL original culture volume. The purified proteorhodopsin was eluted in 5 ml fractions containing 20 mM bis-tris propane, 500 mM imidazole, 0.5 M NaCl, 0.1% DDM, pH 8 at RT. The fractions were combined and concentrated using a 10 kDa cut-off column (Amicon) to OD~10 at the absorption maxima for steady-state Raman and transient absorption experiments or OD~0.05 for fluorescence experiments. Buffer solutions for pH-dependent experiments contained 150 mM NaCl and 2.5% DDM, with 20 mM bis-trispropane (for pH 6.0–7.0) or 20 mM Tris-HCl (for pH 7.5–9.0),.

Steady-state stimulated Raman spectroscopy: Steady-state stimulated Raman experiments were performed as reported previously [3-5], using a 2-mm pathlength quartz cuvette (100-QS, Hellma Analytics).

Femto- to submillisecond transient absorption spectroscopy: Transient absorption measurements were performed with a femtosecond-to-submillisecond pump-probe setup as reported previously [3, 5-7]. The samples were filled in a homemade sample holder that has two 2-mm-thick CaF_2 plates. The sample thickness was set at 400 μm for transient absorption experiments with an appropriate sample spacer. The sample holder was set on a Lissajous scanner forsample refreshment between laser shots with a time interval of 60 seconds between successive exposures to the laser pulses [8]. A CaF_2 plate on a homemade moving stage was used for supercontinuum white light generation, and a selected wavelength region; 400–750 nm, was detected by the photodiode array. The time delay was varied up to 430 μs at 163 data points with the

minimum temporal step of 50 fs. The diameters of the pump and the probe beams at the sample position were ~200 μm and ~50 μm, respectively. The central wavelength and the power of the pump beam were set at 510 nm (~400 nJ), 620 nm (~400 nJ), 670 nm (~400 nJ), and 730 nm (~600 nJ). The instrument response function was ~100 fs, as estimated from global analysis.

Global analysis methodology: Global analysis was performed for the transient absorption spectra using the Glotaran program.[9-10] With global analysis, all wavelengths/wavenumbers were analyzed simultaneously with a set of common time constants [10]. A kinetic model was applied consisting of sequentially interconverting, evolution-associated difference spectra (EADS), *i.e.* $1 \rightarrow 2 \rightarrow 3 \rightarrow \ldots$ in which the arrows indicate successive mono-exponential decays of a time constant, which can be regarded as the lifetime of each EADS [10]. The first EADS corresponds to the difference spectrum at time zero. The first EADS evolves into the second EADS with time constant τ_1, which in turn evolves into the third EADS with time constant τ_2, etc. The procedure clearly visualizes the evolution of the intermediate states of the protein [3, 5, 11]. Decay-associated difference spectra (DADS) indicate the spectral changes with parallel decay channels and independent decay time constants. Intuitively, the DADS provide the difference spectra between the subsequent EADS, provided that the time constants are sufficiently widely separated. It is important to note that the parallel and the sequential analysis are mathematically equivalent and yield identical time constants [12]. The standard errors in the time constants were less than 5% [9, 11].

Fluorescence spectroscopy:

Fluorescence spectra of PR:MMAR at pH 6.0, 6.5, 7.0, 7.5, 8.0 and 8.5 were taken with a Vis/NIR fluorescence spectrometer (Fluoromax, Horiba) at 20°C, as reported previously [13]. For the data acquisition process, the excitation light intensity was monitored by a photodiode and the fluorescence intensity was corrected for the photon flux of the excitation light. The samples were diluted to an OD< 0.05 (per cm) at 760 nm to prevent reabsorption. The pigment concentration was the same for the different pH conditions. The fluorescence quantum yield of PR:MMAR at pH 7.0 with 760-nm excitation was measured using a

near-infrared laser dye (HITCI, Φ_{FL} = 28.3% [14]) dissolved in ethanol as a standard. The samples were contained in a quartz cuvette (104F-QS, Hellma Analytics) with 10-mm pathlength in the excitation direction and 4-mm pathlength in the detection direction. The fluorescence spectra were obtained for the PR:MMAR and HITCI between 700–850 nm, and multi-Gaussian fitting was applied to calculate the total area of emission counts. The fluorescence quantum yield of PR:MAMR ($\Phi_{FL,PR}$) was calculated with the following formula [14]:

$$\Phi_{FL,PR} = \Phi_{FL,dye} \times f_{dye}(\lambda_{ex})/f_{PR}(\lambda_{ex}) \times F_{PR}/F_{dye} \times n_{water}^2/n_{ethanol}^2$$

Here f_x , F_x and n_x represent 1−transmittance, total area of emission and refractive index, respectively.

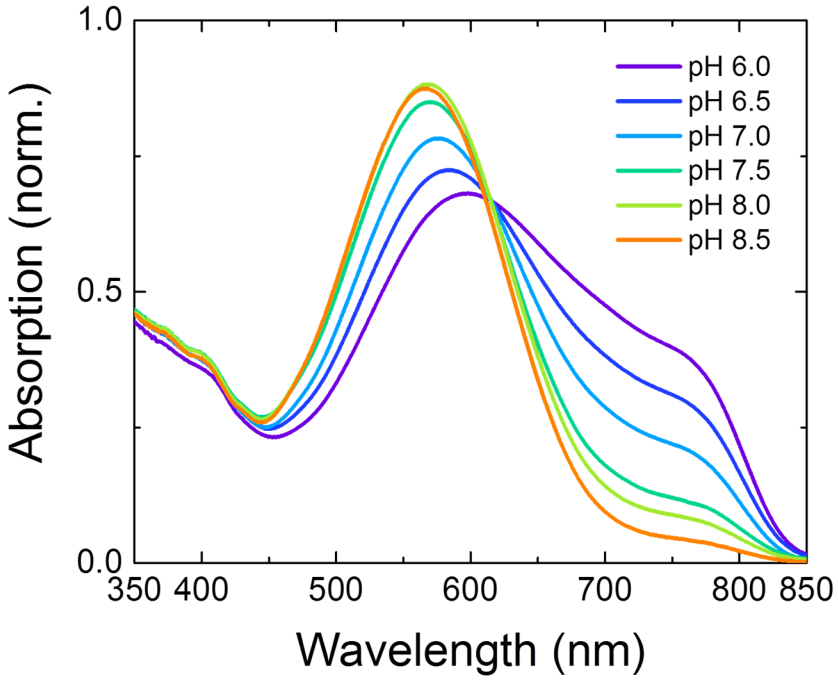

Fig. S1. Normalized pH-dependent absorption spectra of PR:MMAR. Modified from Ganapathy *et al.*(1).

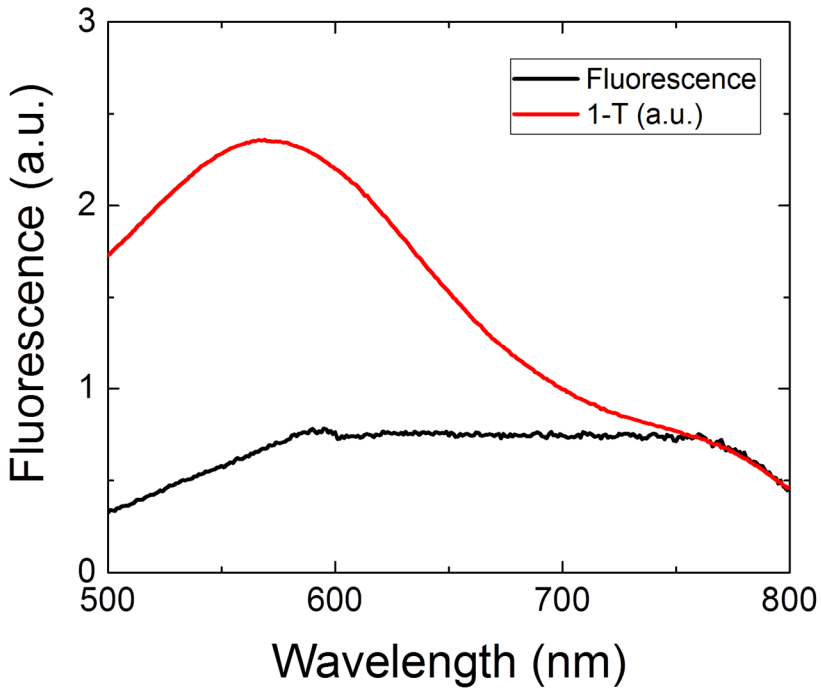

Fig. S2. Fluorescence excitation spectrum of 820-nm fluorescence of PR:MMAR at pH 7.0 overlapped with 1-transmittance (1-T) spectrum.

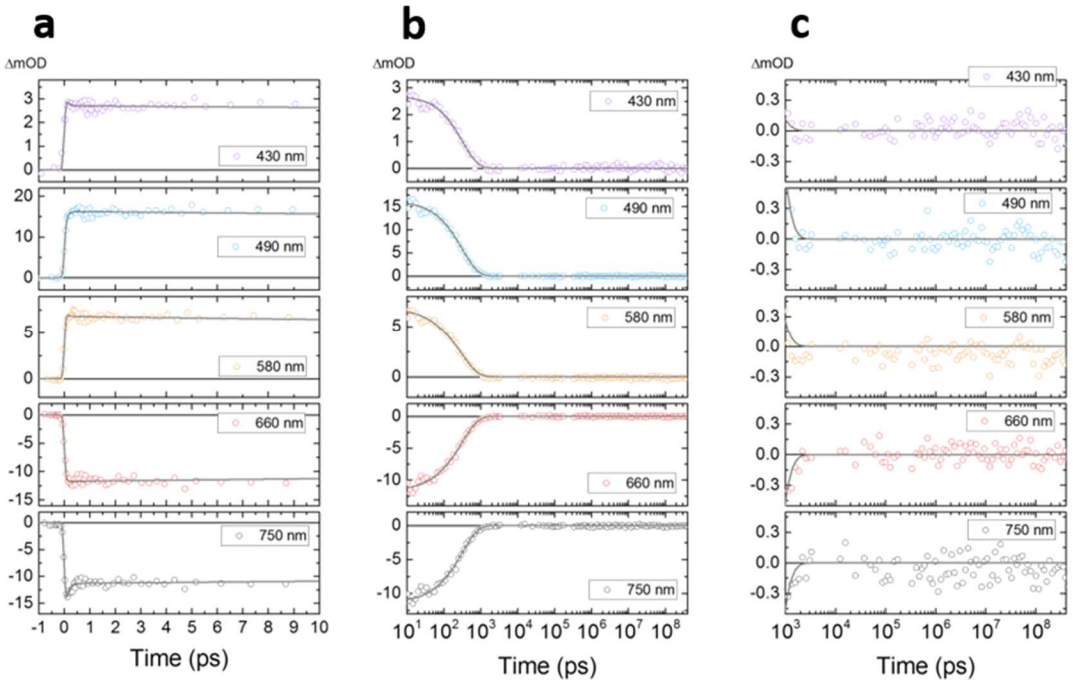

Fig. S3. **Globally-fitted transient absorption data of PR:MMAR at pH 7.0 with 730-nm excitation.**. Selected time traces between (**a**) -1 ps and 10 ps, (**b**) 10 ps and 400 μs and (**c**) 1 ns and 400 μs, at 430, 490, 580, 660 and 750 nm. Open dots show the raw data, and the solid gray lines show fitting curves. For further details see Fig. S7.

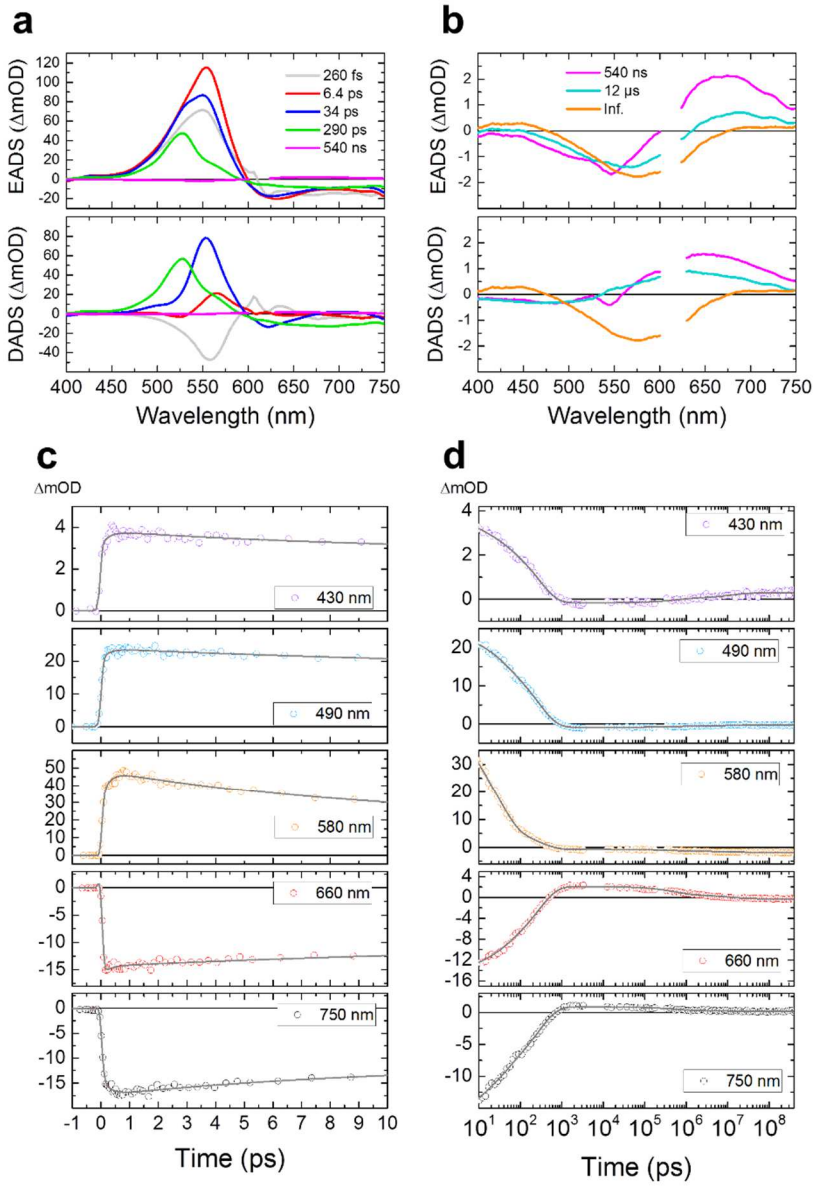

Fig. S4. Globally-fitted transient absorption spectra of PR:MMAR at pH 7.0 with 620-nm excitation. Evolution-associated difference spectra (EADS) and decay-associated difference spectra (DADS) of the (**a**) first five and (**b**) the last three components. In (**b**), the vertical axis has been rescaled and the 540 ns component of panel (**a**) (magenta lines) has been reproduced. The wavelength region of 610–630 nm is omitted because of the strong scattering. Selected time traces between (**c**) -1 ps and 10 ps, and (**d**) 10 ps and 400 µs, at 430, 490, 580, 660 and 750 nm. Open dots show the raw data, and the solid gray lines show fitting curves. The 260 fs component does not involve decay of ground-state bleach/stimulated emission and is assigned to a relaxation process in the excited state. In contrast, the 6.4, 34 and 290 ps lifetimes clearly represent loss of ground-state bleach/stimulated emission and hence are due to excited-state decay. Note that the 290 ps EADS and DADS (green lines in panel (**a**) are nearly identical to the 310 ps EADS/DADS upon 730 nm excitation (**Fig S3(a)**, blue lines), indicating that this component arises from a fraction of directly excited 760-nm species that has a residual absorption at the 620 nm excitation wavelength. We conclude that the effective fluorescence lifetime is significantly shorter at 620 nm

excitation than at 730 nm excitation. In addition, a K-like photo-isomerization product with an absorption at 670 nm is observed at low amplitude (panel **(a, b)** magenta line) implying that isomerization occurs at a low yield with this excitation wavelength. The K-like photoproduct evolves in 540 ns and 12 μs into an M-like intermediate (panel (**b**), orange line) that has an absorption around 420 nm and is a marker of a deprotonated retinylidene Schiff-base (RSB)[15], indicating proton transfer from the protonated RSB, most likely to the counterion Asp97, consistent with the observation that PR:MMAR is capable of pumping protons[2]. For further details see Fig. S7.

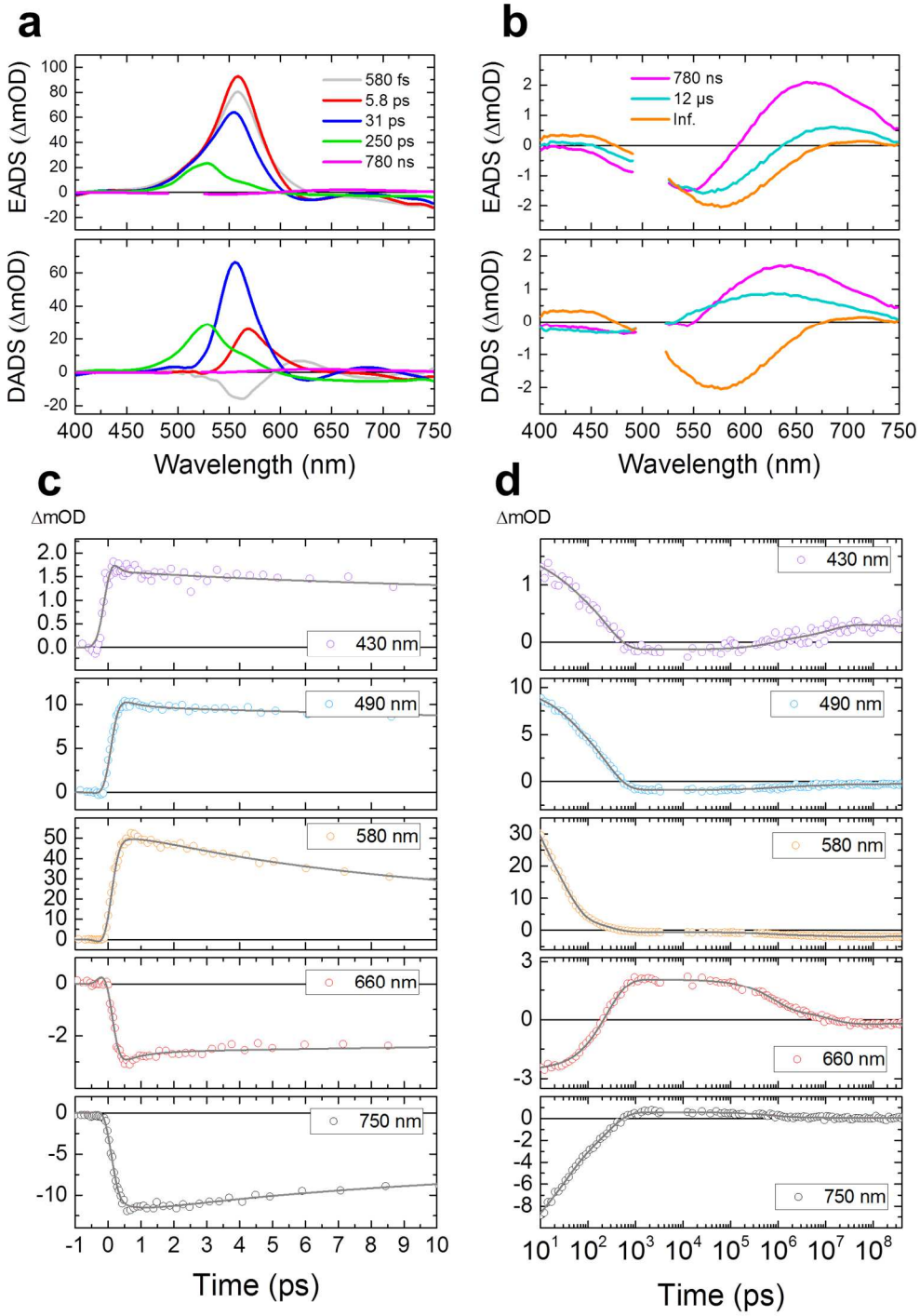

Fig. S5. Global-fitted transient absorption spectra of PR:MMAR at pH 7.0 with 510-nm excitation. Evolution-associated difference spectra (EADS) and decay-associated difference spectra (DADS) of the (**a**) first five and (**b**) the last three components. In (**b**), the vertical axis has been rescaled and the 540 ns component of panel (**a**) (magenta lines) has been reproduced. The wavelength region of 500–520 nm is omitted because of the strong scattering. Selected time traces between (**c**) -1 ps and 10 ps, and (**d**) 10 ps

and 400 μs, at 430, 490, 580, 660 and 750 nm. Open dots show the raw data, and the solid gray lines show fitting curves. For further details see Fig. S7.

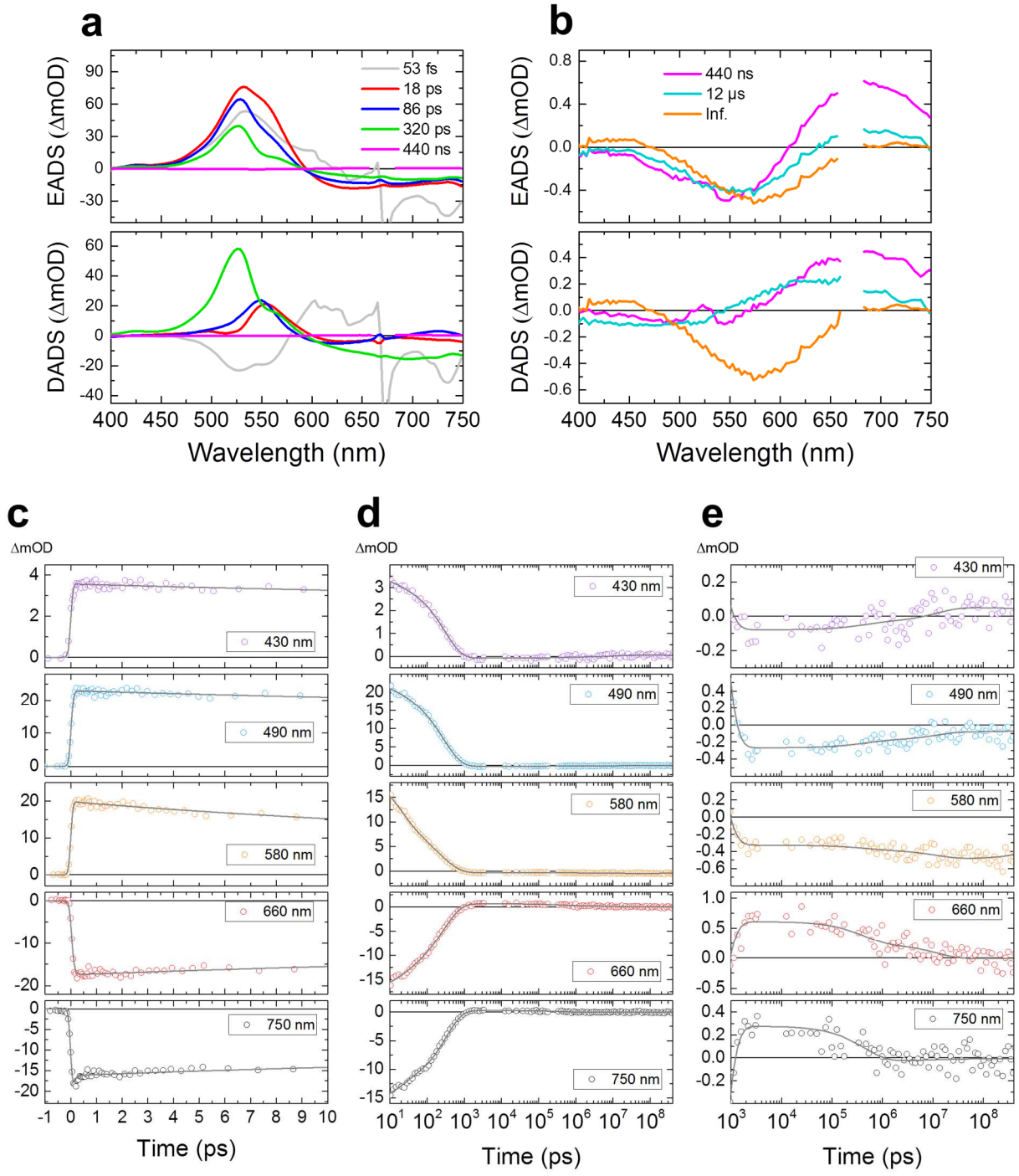

Fig. S6. Global-fitted transient absorption spectra of PR:MMAR at pH 7.0 with 670-nm excitation. Evolution-associated difference spectra (EADS) and decay-associated difference spectra (DADS) of the (**a**) first five and (**b**) the last three components. In (**b**), the vertical axis has been rescaled and the 540 ns component of panel (**a**) (magenta lines) has been reproduced. The wavelength region of 660–680 nm is omitted because of the strong scattering. Selected time traces between (**c**) -1 ps and 10 ps, (**d**) 10 ps and 400 µs and (**e**) 1 ns and 400 µs, at 430, 490, 580, 660 and 750 nm. Open dots show the raw data, and the solid gray lines show fitting curves. For further details see Fig. S7.

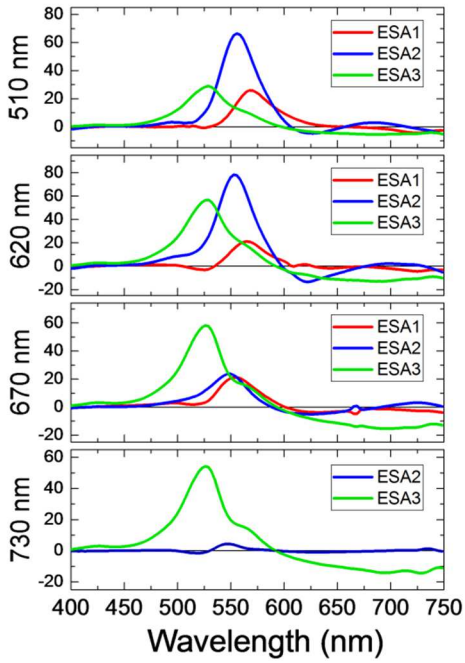

Excitation wavelength	ESA1	ESA2	ESA3	K-like state
510 nm	26	**66**	29	**2.1**
620 nm	21	**78**	56	**2.1**
670 nm	21	**24**	58	**0.6**
730 nm	—	4	54	—

Fig. S7. DADS of the three excited-state components of PR:MMAR at pH 7.0 with excitation at 510, 620, 670 and 730 nm. ESA1, ESA2 and ESA3 show the excited-state component decaying in ≲10 ps, ~30 ps and ~300 ps, respectively. The table shows comparison of the peak intensities of the excited-state absorption species and the K-like state of PR:MMAR with different excitation wavelengths. The unit of the values is mOD. In the graphs, the DADS of the ESA1, ESA2 and ESA3 with different excitation wavelengths (510, 620, 670 and 730 nm) are shown. The populations of ESA1 were almost identical with excitation at 510, 620 and 670 nm, while those of ESA2 are about 3-fold smaller with 670-nm excitation as compared with 510- and 620-nm excitation. Strikingly, the K-like state population is also ~3-fold smaller with 670-nm excitation than with 510- and 620-nm excitation, which is suggestive of a positive correlation between the population of ESA2 and that of the K-like photoproduct. These observations indicate that ESA2 is the productive excited-state species, and ESA1 is a non-productive state. Overall, we conclude that the ESA2 is the dominant state in producing the K-like intermediate in ~30 ps, and the ESA1 and ESA3 are excited-state species returning to the initial ground state. It should be noted that it is not clear whether proton transfer from the protonated RSB in PR:MMAR is essential for its proton pumping function.[16]

References

(1) Ganapathy, S.; Becheau, O.; Venselaar, H.; Frolich, S.; van der Steen, J. B.; Chen, Q.; Radwan, S.; Lugtenburg, J.; Hellingwerf, K. J.; de Groot, H. J.; de Grip, W. J. Modulation of spectral properties and pump activity of proteorhodopsins by retinal analogues. *Biochem. J.* **2015,** *467*, 333-43.
(2) Ganapathy, S.; Venselaar, H.; Chen, Q.; de Groot, H. J.; Hellingwerf, K. J.; de Grip, W. J. Retinal-based proton pumping in the near infrared. *J. Am. Chem. Soc.* **2017,** *139*, 2338-2344.
(3) Hontani, Y.; Inoue, K.; Kloz, M.; Kato, Y.; Kandori, H.; Kennis, J. T. The photochemistry of sodium ion pump rhodopsin observed by watermarked femto- to submillisecond stimulated Raman spectroscopy. *Phys. Chem. Chem. Phys*. **2016,** *18*, 24729-36.
(4) Kloz, M.; Weissenborn, J.; Polivka, T.; Frank, H. A.; Kennis, J. T. M. Spectral watermarking in femtosecond stimulated Raman spectroscopy: resolving the nature of the carotenoid S-star state. *Phys. Chem. Chem. Phys*. **2016,** *18*, 14619-14628.
(5) Hontani, Y.; Marazzi, M.; Stehfest, K.; Mathes, T.; van Stokkum, I. H. M.; Elstner, M.; Hegemann, P.; Kennis, J. T. M. Reaction dynamics of the chimeric channelrhodopsin C1C2. *Sci. Rep.* **2017,** *7*, 7217.
(6) Ravensbergen, J.; Abdi, F. F.; van Santen, J. H.; Frese, R. N.; Dam, B.; van de Krol, R.; Kennis, J. T. M. Unraveling the Carrier Dynamics of BiVO4: A Femtosecond to microsecond transient absorption study. *J. Phys. Chemi. C* **2014,** *118*, 27793-27800.
(7) Berera, R.; van Grondelle, R.; Kennis, J. T. M. Ultrafast transient absorption spectroscopy: principles and application to photosynthetic systems. *Photosynth. Res*. **2009,** *101*, 105-118.
(8) Alexandre, M. T.; Domratcheva, T.; Bonetti, C.; van Wilderen, L. J.; van Grondelle, R.; Groot, M. L.; Hellingwerf, K. J.; Kennis, J. T. Primary reactions of the LOV2 domain of phototropin studied with ultrafast mid-infrared spectroscopy and quantum chemistry. *Biophys. J.* **2009,** *97*, 227-37.
(9) Snellenburg, J. J.; Laptenok, S. P.; Seger, R.; Mullen, K. M.; van Stokkum, I. H. M. Glotaran: A Java-based graphical user interface for the R package TIMP. *J. Statist. Softw.* **2012,** *49*, 1-22.
(10) van Stokkum, I. H. M.; Larsen, D. S.; van Grondelle, R. Global and target analysis of time-resolved spectra. *Biochim. Biophys. Acta* **2004,** *1657*, 82-104.
(11) Kennis, J. T. M.; Groot, M. L. Ultrafast spectroscopy of biological photoreceptors. *Curr. Opin. Struct. Biol.* **2007,** *17*, 623-630.
(12) Toh, K. C.; Stojkovic, E. A.; van Stokkum, I. H.; Moffat, K.; Kennis, J. T. Fluorescence quantum yield and photochemistry of bacteriophytochrome constructs. *Phys. Chem. Chem. Phys*. **2011,** *13*, 11985-97.
(13) Hontani, Y.; Shcherbakova, D. M.; Baloban, M.; Zhu, J.; Verkhusha, V. V.; Kennis, J. T. Bright blue-shifted fluorescent proteins with Cys in the GAF domain engineered from bacterial phytochromes: fluorescence mechanisms and excited-state dynamics. *Sci. Rep.* **2016,** *6*, 37362.
(14) Rurack, K.; Spieles, M. Fluorescence quantum yields of a series of red and near-infrared dyes emitting at 600-1000 nm. *Anal. Chem.* **2011,** *83*, 1232-42.
(15) Ernst, O. P.; Lodowski, D. T.; Elstner, M.; Hegemann, P.; Brown, L. S.; Kandori, H. Microbial and animal rhodopsins: structures, functions, and molecular mechanisms. *Chem. Rev.* **2014,** *114*, 126-63.
(16) Xiao, Y. W.; Partha, R.; Krebs, R.; Braiman, M. Time-resolved FTIR spectroscopy of the photointermediates involved in fast transient H+ release by proteorhodopsin. *J. Phys. Chem. B* **2005,** *109*, 634-641.